Microstructure and Spectral selectivity of Pt-Al_2O_3 nanocoatings for high temperature applications

Z Y Nuru[1-2], S Khamlich[1], K. Roro[1], T F G Muller[2], C J Arendse[2] & M Maaza[1-3]
[1]Nanosciences African Network, MRD-iThemba Labs, National Research Foundation, Old Faure road, Somerset West, South Africa
[2]Dept. of Physics, University of Western Cape, Private Bag x 17, Belleville, 17, Belleville, South Africa
[3]Faculty of Sciences, Pretoria-Tshwane University of Technology, Private Bag X 680, Pretoria, South Africa.
E-mail: zebib@tlabs.ac.za

Abstract. In terms of high photo-thermal conversion efficiency and thermal stability, multilayered structures based on metal-dielectric composites i.e. ceramic-metal (cermets) are the most attractive candidates for receivers operating at high temperature (above 400°C). Pt-Al_2O_3 cermet nano-composites are a representative family as per their high temperature chemical inertness and stability. This contribution reports on the microstructure and optical property of Pt-Al_2O_3 cermet nano-composites deposited in a multilayered tandem structure. The radio-frequency sputtered Pt-Al_2O_3 cermet consisting of stainless steel substrate/ Mo coating layer/ Pt-Al_2O_3 absorbing layer /Al_2O_3 protective layer and stainless steel substrate/ Mo coating layer /Pt-Al_2O_3 absorbing layer for different composition and thickness of Pt-Al_2O_3 coatings. This optimized coating exhibits high solar absorptance (α ~0.95/0.93) and low thermal emittance (ϵ ~0.11/0.17 at 89 °C) with and without Al_2O_3 protecting layer, respectively, which are stable up to 650°C in air. X-ray diffraction, atomic force microscopy, effective medium theory and UV-VIS-NIR total reflectance were used to characterize the microstructure, morphology, theoretical modeling and optical property of these coatings.

1. Introduction

Solar collectors are environmentally friendly and non-polluting technological way of converting solar radiations into thermal energy to fulfil the ever the current increasing demand of energy supply [1]. Basically, a solar collector's photo-thermal conversion efficiency depends on the solar selective absorbing coating. A variety of selective absorbers have been proposed and fabricated for photo-thermal applications [1-3]. Selective absorbing surfaces can be classified into three main types from a structural point of view: (i) intrinsic, (ii) optical trapping surface and (iii) tandem. Tandem selective surfaces can further be classified into three: (i) semiconductor-metal tandems (ii) multilayered absorbers, and (iii) metal – dielectric composite tandem. An intrinsic solar absorbing material is wavelength selective. However, there is no naturally occurring absorbing material. Optical trapping surfaces can produce high solar absorptance by multiple reflections among them one could quote needle-like, dendritic, or porous microstructures. Tandem absorbers consist of at least two layers with different optical properties: Semiconductor-metal tandems absorb short wavelength radiation because of the semiconductor band gap and have low thermal emittance as a result of the metal layer. Multilayered absorbers use multiple reflections between layers to absorb light and can be tailored to be efficient selective absorbers. Metal-dielectric composites called cermets type of solar absorbers exhibit high absorption as well as high reflection in the UV-VIS and NIR respectively over a large solar

spectrum range. In addition, when such a composite cermet-coating is formed on a highly reflecting metal surface, the resulting tandem coating has a good spectral selectivity [4-7]. Concerning the fabrication of such solar absorbers, several techniques such as electroplating, physical vapour deposition, chemical vapour deposition and so on, have been developed to produce spectrally selective absorbing surfaces. However, among these sputtering approach is one of physical vapour deposition which is the most commonly and widely used [4-12]. The optical properties of such composites can be intermediated between those of metals and of the dielectric. Effective dielectric permeability of the composite, which can be related to the constituents in the effective medium theories, can be used to estimate the optical performance of the cermet. This contribution reports on the optimization and further selectivity improvement of radio-frequency sputtered graded Pt-Al_2O_3 deposited onto a Mo base layer exhibiting a high solar absorptance and low thermal emittance with a significant thermal stability up to 650°C in air with and without antireflection layers.

2. Experiments and synthesis

Al_2O_3 disc "~13 cm in Ø" with circular small Pt pellets "~5 mm in Ø" placed on it was used as a target. The Pt pellets were placed in a hexagonal array on the Al_2O_3 disc target to ensure an isotropic deposition of Pt and Al_2O_3. The composition of the films was varied according to the number of Pt pellets used. The optimized working pressure was fixed to ~10^{-2} Torr without heating the samples' stainless steel substrates as was substantiated by early studies on pure Pt-Al_2O_3 samples [7-11]. The optimized synthesized cermet samples were characterized from morphological, crystallographic and optical view points by using scanning electron microscopy "SEM", atomic force microscopy "AFM", X-rays diffraction "XRD". Total reflectance was collected by an integrated sphere system, that includes both specular and non-specular components, was measured with a double beam Vary Cary 500 spectrophotometer to calculate how Pt-Al_2O_3 cermet films absorb light using an AM1.5 and a direct measurement of emittance *using* an emissometer model AE1 which has an accuracy of about ± 0.01 emittance units was used to measure the emissivity of the devices.

3. Results and discussions

The optimized Pt concentration in the Pt-Al_2O_3 cermet layer i.e. in terms of the Pt filling factor "*f* value", was deduced by modeling using the Brugeman effective medium approximation. The Pt-Al_2O_3 cermet layer was treated as an isotropic inhomogeneous medium with a random mixture of metallic Pt nano-particles in the host dielectric matrix with a filling factor *f* and dielectric constants ϵ_{pt} and ϵ_{Al2O3} as a homogeneous medium with an effective dielectric constant ϵ_{eff} given by:

$$\epsilon = f\left(\frac{\epsilon_{pt} - \epsilon_{eff}}{\epsilon_{pt} + 2\epsilon_{eff}}\right) + (1-f)\left(\frac{\epsilon_{Al2O3} - \epsilon_{eff}}{\epsilon_{Al2O3} + 2\,\epsilon_{eff}}\right) \quad (1)$$

Using the tabulated values of ϵ_{Pt} and ϵ_{Al2O3} from the standard Palik's database, the preliminary modeling calculations allowed the determination of the value of the Pt filling factor "*f*" at about ~0.34 and the effective optical constants (refractive index, n and extinction coefficient, k) given by:

$$n^2 = \left(\frac{\sqrt{\epsilon_{pt}^{\,2} + \epsilon_{Al2O3}^{\,2}}}{2} + \frac{\epsilon_{pt}}{2}\right) \quad (2)$$

and

$$k^2 = \left(\frac{\sqrt{\epsilon_{pt}^{\,2} + \epsilon_{Al2O3}^{\,2}}}{2} - \frac{\epsilon_{pt}}{2}\right) \quad (3)$$

As reported in Figure 1, the simulation demonstrates a prominent feature of the optical constants calculated from the above equation that illustrated how the Pt-Al_2O_3 composite changed the optical constants from the constituents: Pt and Al_2O_3. Moreover, it indicates that the effective refractive index was greater than the extinction coefficient while both of them were positive. This indicates that, in the UV-VIS-NIR spectral region, light was not rejected but absorbed. In case of equivalent coatings of pure Pt and Al_2O_3, the light would be reflected and transmitted respectively. The optimized Pt-Al_2O_3 thin film thickness was found to be about ~70 nm with a Mo buffer layer of ~150 nm onto the considered stainless steel substrates.

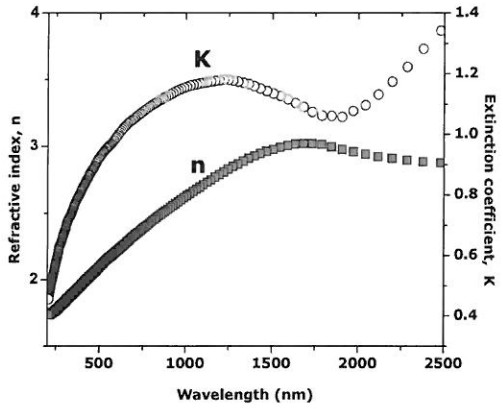

Figure 1. Optical constants of Pt-Al_2O_3 composite calculated using Bruggeman model. The Pt filling factor in the Pt-Al_2O_3 cermet coatings was ~0.34.

Figure 2 reports a typical SEM surface morphology of Pt-Al_2O_3 thin film/Mo buffer layer/stainless steel substrate with f~0.34. The corresponding cermet film exhibits a tortuous surface morphology with Pt nano-particles distributed isotropically in the basal plane indicated by the arrows. Their average diameter and inter-particles distance were statistically about 4-6 nm and 7-10 nm respectively.

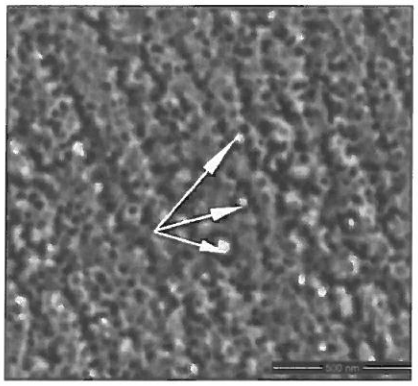

Figure 2. Scanning electron microscopy of the optimized cermet sample: anti-reflecting layer of ~ 110 nm Al_2O_3/ ~70 nm Pt-Al_2O_3/~150 nm Mo/~0.5 mm Stainless steel substrate.

Figure 3 depicts a representative AFM surface scanning of the cermet sample's surface exhibits two type of surface topographies; highly disordered and semi-ordered stripes type zones. These latter regions of semi-disordered "stripes" have an average length of ~0.41 nm consisting of 1-D chains-like of length of about ~0.41 nm. This 1-D chains-like were spatially ordered and consisted of crystallites with an average diameter of about 250 nm. The crystallites, in the disordered regions have approximately an identical average size. The average roughness value was of about 8.81 nm. Relatively speaking, this roughness value was comparable to the average diameter and inter-particles distance which were found to be about 4-6 nm and 7-10 nm respectively. Hence, one could deduce that the surface topography was controlled by the Pt nano-particles.

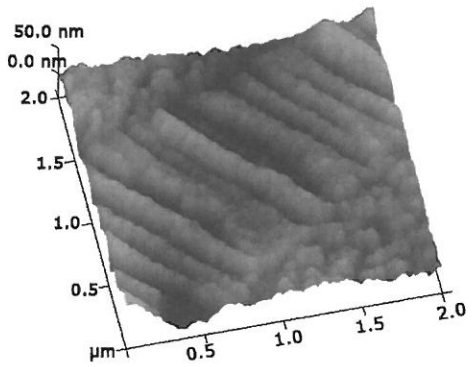

Figure 3. Atomic force microscopy topography of the optimized cermet sample: anti-reflecting layer of ~110 nm Al_20_3/~70 nm Pt-Al_2O_3/~150 nm Mo/~0.5 mm Stainless steel substrate.

Figure 4 reports the crystallographic orientations of the optimized Al_2O_3/Pt-Al_2O_3/Mo/Stainless steel. Taking into account the anti-reflecting layer of Al_20_3, cermet layer of Pt-Al_2O_3 as well as the buffer IR reflective metallic layer of Mo is thin; the probing X-rays impinging the samples do penetrate and reach the stainless steel substrate. Indeed as shown by Figure 4, while the stainless steel substrate was highly crystalline with a net (111), (200) and (220) texturing, the buffer IR reflecting layer of Mo as well as the host Al_2O_3 matrix seemed to be fully amorphous as there was no corresponding Bragg peaks in the recorded 2Θ angular range of 30-80 deg. In contrast, and within the same angular range, one observes the (111), (200) and (220) Pt Bragg peaks. These peaks were quite wide corresponding to Pt grains with an average size "using the Debye-Scherer approximation" of about 3.2-4.7 nm in diameter hence corroborating with the values deduced from the SEM and AFM investigations within the error bars.

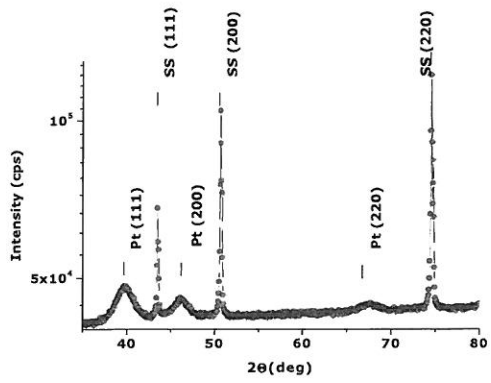

Figure 4. X rays diffraction patterns of the optimized cermet samples with and without the anti-reflecting layer of ~110 nm Al_2O_3/~70 nm Pt-Al_2O_3/~150 nm Mo/~0.5 mm Stainless steel substrate.

The optical reflectance spectra of simulated and experimental Pt-Al_2O_3 composites in the UV-VIS-NIR range of 300-2500 nm in particular for the Pt- Al_2O_3/Mo/Stainless steel substrate tandems without and with Al_2O_3 antireflection layer are shown in figure 5 (a) and (b) respectively. Hence the tandem without the Al_2O_3 anti-reflecting layer exhibited an absorptance of 0.93 and thermal emittance of 0.17, the corresponding one of the tandem with the Al_2O_3 anti-reflecting layer obtained an absorptance of 0.95 and thermal emittance of 0.11. The average total reflectance in the first spectral region was less than 10% it was decreased to 5% in the second one. These very low total reflectance values, which demonstrate the feasibility of the current considered optimized cermet based tandems, should be attributed not only to the optimized nature of the tandems with or without the Al_2O_3 reflecting layer but to the specific surface morphology and texture of these coatings as well.

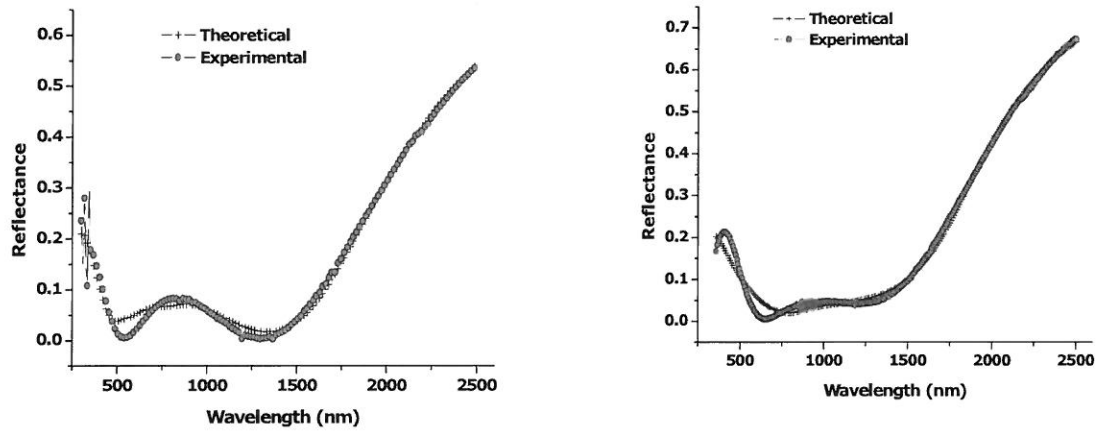

Figure 5. a) Experimental and calculated total Reflectivities "specular + non sepcular" of the optimized cermet samples without anti-reflection layer of ~70 nm Pt- Al_2O_3/~150 nm Mo/~0.5 mm Stainless steel substrate. **b)** Experimental and calculated total Reflectivities "specular+ non sepcular" of the optimized cermet samples with anti-reflecting layer of ~110 nm Al_2O_3/~70 nm Pt- Al_2O_3/~150 nm Mo/~0.5 mm Stainless steel substrate.

4. Conclusion

In this work, optimized multilayered Pt-Al_2O_3 cermet nano-coatings onto Mo IR reflecting buffer layer coated stainless steel substrate with and without anti-reflecting layers of Al_2O_3 exhibited an excellent spectral selectivity of 0.95/0.11 which was consistent with a computer simulation. These cermet films are found to be thermally stable up to 650 °C in air. Combining such superior optical properties and the refractory nature of alumina as well as the chemical inertness of Pt, this type of coatings are competitive candidates for high temperature solar power plant applications.

Acknowledgment

We would like to thank for the finance support from (i) the Organization of Women Scientists for Developing World-Trieste "OWSDW", the Abdus Salam ICTP-Trieste, the Nanosciences African Network "NANOAFNET"-Cape Town, as well as iThemba LABS-National Research Foundation of South Africa.

References

[1] Granqvist C G 1991 J. Appl. Phys. A **52** 83
[2] Granqvist C G and Niklasson G A 1978 Phys. Rev. B **18** 554
[3] Niklasson G A and C G Granqvist 1984 J. Appl. Phys. **55** 3382
[4] Sella C and Lafait J 1988 J. Appl. Surf. Sci. **33/34** 942
[5]. Kenndy C E 2002 NREL/TP-520-31267
[6]. Thronton J A, Penfold A S and Lamb J L 1980 Thin Solid Films **72** 101
[7]. Berthier S, Lafait J, Sella C and Vien T K 1985 Thin Solid Films **125** 171
[8]. Maaza M, Nemraoui O, Sella C , Lafait J, Gibaud A, Pischedda V 2005 J. Phys. Letters A **344**
[9]. Sella C, Maaza M, Pardo B, Dunsteter F and Sainte Catherine M C 1997 J. Phys. A **241** 192
[10]. Gibaud A, Sella C, Maaza M, Sung L, Dura J A, Satija S.K 1999 Thin Solid Films **340** 153
[11]. Sella C, Maaza M, Pardo B, Dunsteter F, Martin J C and Kaba A 1997 J. Surface and Coatings Technology **97** 603
[12]. Maaza M, Nemraoui O, Sella C, Lafait J, Gibaud A, Baruch-Barak A and Beye A C 2006 J. Solid State Comms. **137** 166

IJP/678394

Invoice

Hindawi

Article Processing Charges for Article to be Published in	Volume
International Journal of Photoenergy	2012

Date	Invoice Number	Terms
27 March 2012	IJP/678394	Payable Upon Receipt

Bill to

Kittessa Roro, Bonex Mwakikunga, Brian Yalisi, Tile Ngcali and Andrew Forbes
South Africa

Article Title	Total Charge
Effect of accelerated thermal ageing on the selective solar thermal harvesting properties of multiwall carbon nanotube/nickel oxide nanocomposite coatings	$800

Check Payment	Please make check payable to "Hindawi Publishing Corporation" and mail it to:	Hindawi Publishing Corporation 410 Park Avenue 15th Floor, #287 pmb New York, NY 10022 USA
Online Payment	To pay online please use the following link:	Http://www.hindawi.com/apc.aspx?n=678394

SN:

Microstructure and Spectral selectivity of Pt-Al_2O_3 nanocoatings for high temperature applications

Z Y Nuru[1-2], S Khamlich[1], K. Roro[1], T F G Muller[2], C J Arendse[2] & M Maaza[1-3]
[1]Nanosciences African Network, MRD-iThemba Labs, National Research Foundation, Old Faure road, Somerset West, South Africa
[2]Dept. of Physics, University of Western Cape, Private Bag x 17, Belleville, 17, Belleville, South Africa
[3]Faculty of Sciences, Pretoria-Tshwane University of Technology, Private Bag X 680, Pretoria, South Africa.
E-mail: zebib@tlabs.ac.za

Abstract. In terms of high photo-thermal conversion efficiency and thermal stability, multilayered structures based on metal-dielectric composites i.e. ceramic-metal (cermets) are the most attractive candidates for receivers operating at high temperature (above 400°C). Pt-Al_2O_3 cermet nano-composites are a representative family as per their high temperature chemical inertness and stability. This contribution reports on the microstructure and optical property of Pt-Al_2O_3 cermet nano-composites deposited in a multilayered tandem structure. The radio-frequency sputtered Pt-Al_2O_3 cermet consisting of stainless steel substrate/ Mo coating layer/ Pt-Al_2O_3 absorbing layer /Al_2O_3 protective layer and stainless steel substrate/ Mo coating layer /Pt-Al_2O_3 absorbing layer for different composition and thickness of Pt-Al_2O_3 coatings. This optimized coating exhibits high solar absorptance (α ~0.95/0.93) and low thermal emittance (ϵ ~0.11/0.17 at 89 °C) with and without Al_2O_3 protecting layer, respectively, which are stable up to 650°C in air. X-ray diffraction, atomic force microscopy, effective medium theory and UV-VIS-NIR total reflectance were used to characterize the microstructure, morphology, theoretical modeling and optical property of these coatings.

1. Introduction

Solar collectors are environmentally friendly and non-polluting technological way of converting solar radiations into thermal energy to fulfil the ever the current increasing demand of energy supply [1]. Basically, a solar collector's photo-thermal conversion efficiency depends on the solar selective absorbing coating. A variety of selective absorbers have been proposed and fabricated for photo-thermal applications [1-3]. Selective absorbing surfaces can be classified into three main types from a structural point of view: (i) intrinsic, (ii) optical trapping surface and (iii) tandem. Tandem selective surfaces can further be classified into three: (i) semiconductor-metal tandems (ii) multilayered absorbers, and (iii) metal – dielectric composite tandem. An intrinsic solar absorbing material is wavelength selective. However, there is no naturally occurring absorbing material. Optical trapping surfaces can produce high solar absorptance by multiple reflections among them one could quote needle-like, dendritic, or porous microstructures. Tandem absorbers consist of at least two layers with different optical properties: Semiconductor-metal tandems absorb short wavelength radiation because of the semiconductor band gap and have low thermal emittance as a result of the metal layer. Multilayered absorbers use multiple reflections between layers to absorb light and can be tailored to be efficient selective absorbers. Metal-dielectric composites called cermets type of solar absorbers exhibit high absorption as well as high reflection in the UV-VIS and NIR respectively over a large solar

spectrum range. In addition, when such a composite cermet-coating is formed on a highly reflecting metal surface, the resulting tandem coating has a good spectral selectivity [4-7]. Concerning the fabrication of such solar absorbers, several techniques such as electroplating, physical vapour deposition, chemical vapour deposition and so on, have been developed to produce spectrally selective absorbing surfaces. However, among these sputtering approach is one of physical vapour deposition which is the most commonly and widely used [4-12]. The optical properties of such composites can be intermediated between those of metals and of the dielectric. Effective dielectric permeability of the composite, which can be related to the constituents in the effective medium theories, can be used to estimate the optical performance of the cermet. This contribution reports on the optimization and further selectivity improvement of radio-frequency sputtered graded Pt-Al_2O_3 deposited onto a Mo base layer exhibiting a high solar absorptance and low thermal emittance with a significant thermal stability up to 650°C in air with and without antireflection layers.

2. Experiments and synthesis

Al_2O_3 disc "~13 cm in Ø" with circular small Pt pellets "~5 mm in Ø" placed on it was used as a target. The Pt pellets were placed in a hexagonal array on the Al_2O_3 disc target to ensure an isotropic deposition of Pt and Al_2O_3. The composition of the films was varied according to the number of Pt pellets used. The optimized working pressure was fixed to ~10^{-2} Torr without heating the samples' stainless steel substrates as was substantiated by early studies on pure Pt-Al_2O_3 samples [7-11]. The optimized synthesized cermet samples were characterized from morphological, crystallographic and optical view points by using scanning electron microscopy "SEM", atomic force microscopy "AFM", X-rays diffraction "XRD". Total reflectance was collected by an integrated sphere system, that includes both specular and non-specular components, was measured with a double beam Vary Cary 500 spectrophotometer to calculate how Pt-Al_2O_3 cermet films absorb light using an AM1.5 and a direct measurement of emittance *using* an emissometer model AE1 which has an accuracy of about ± 0.01 emittance units was used to measure the emissivity of the devices.

3. Results and discussions

The optimized Pt concentration in the Pt-Al_2O_3 cermet layer i.e. in terms of the Pt filling factor "*f* value", was deduced by modeling using the Brugeman effective medium approximation. The Pt-Al_2O_3 cermet layer was treated as an isotropic inhomogeneous medium with a random mixture of metallic Pt nano-particles in the host dielectric matrix with a filling factor *f* and dielectric constants ϵ_{pt} and ϵ_{Al2O3} as a homogeneous medium with an effective dielectric constant ϵ_{eff} given by:

$$\epsilon = f\left(\frac{\epsilon_{pt} - \epsilon_{eff}}{\epsilon_{pt} + 2\epsilon_{eff}}\right) + (1-f)\left(\frac{\epsilon_{Al2O3} - \epsilon_{eff}}{\epsilon_{Al2O3} + 2\,\epsilon_{eff}}\right) \quad (1)$$

Using the tabulated values of ϵ_{Pt} and ϵ_{Al2O3} from the standard Palik's database, the preliminary modeling calculations allowed the determination of the value of the Pt filling factor "*f*" at about ~0.34 and the effective optical constants (refractive index, n and extinction coefficient, k) given by:

$$n^2 = \left(\frac{\sqrt{\epsilon_{pt}{}^2 + \epsilon_{Al2O3}{}^2}}{2} + \frac{\epsilon_{pt}}{2}\right) \quad (2)$$

and

$$k^2 = \left(\frac{\sqrt{\epsilon_{pt}{}^2 + \epsilon_{Al2O3}{}^2}}{2} - \frac{\epsilon_{pt}}{2}\right) \quad (3)$$

As reported in Figure 1, the simulation demonstrates a prominent feature of the optical constants calculated from the above equation that illustrated how the Pt-Al_2O_3 composite changed the optical constants from the constituents: Pt and Al_2O_3. Moreover, it indicates that the effective refractive index was greater than the extinction coefficient while both of them were positive. This indicates that, in the UV-VIS-NIR spectral region, light was not rejected but absorbed. In case of equivalent coatings of pure Pt and Al_2O_3, the light would be reflected and transmitted respectively. The optimized Pt-Al_2O_3 thin film thickness was found to be about ~70 nm with a Mo buffer layer of ~150 nm onto the considered stainless steel substrates.

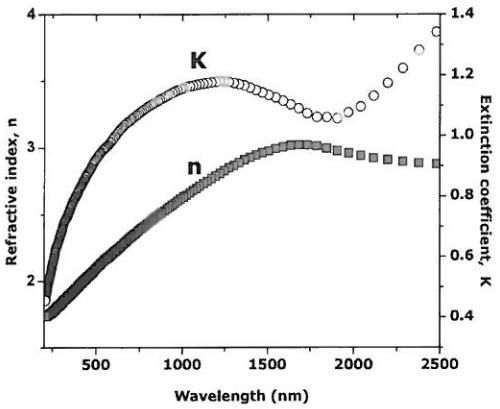

Figure 1. Optical constants of Pt-Al_2O_3 composite calculated using Bruggeman model. The Pt filling factor in the Pt-Al_2O_3 cermet coatings was ~0.34.

Figure 2 reports a typical SEM surface morphology of Pt-Al_2O_3 thin film/Mo buffer layer/stainless steel substrate with f~0.34. The corresponding cermet film exhibits a tortuous surface morphology with Pt nano-particles distributed isotropically in the basal plane indicated by the arrows. Their average diameter and inter-particles distance were statistically about 4-6 nm and 7-10 nm respectively.

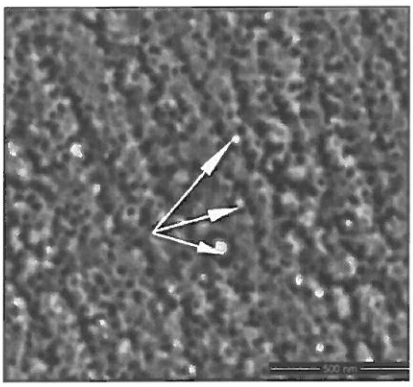

Figure 2. Scanning electron microscopy of the optimized cermet sample: anti-reflecting layer of ~ 110 nm Al_2O_3/ ~70 nm Pt-Al_2O_3/~150 nm Mo/~0.5 mm Stainless steel substrate.

Figure 3 depicts a representative AFM surface scanning of the cermet sample's surface exhibits two type of surface topographies; highly disordered and semi-ordered stripes type zones. These latter regions of semi-disordered "stripes" have an average length of ~0.41 nm consisting of 1-D chains-like of length of about ~0.41 nm. This 1-D chains-like were spatially ordered and consisted of crystallites with an average diameter of about 250 nm. The crystallites, in the disordered regions have approximately an identical average size. The average roughness value was of about 8.81 nm. Relatively speaking, this roughness value was comparable to the average diameter and inter-particles distance which were found to be about 4-6 nm and 7-10 nm respectively. Hence, one could deduce that the surface topography was controlled by the Pt nano-particles.

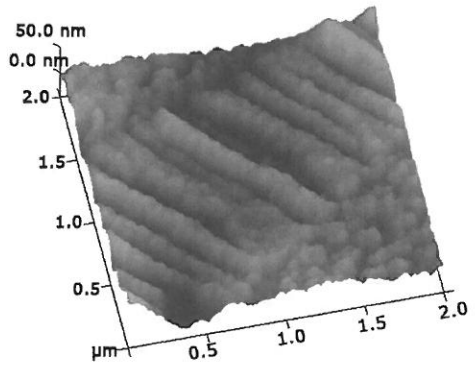

Figure 3 . Atomic force microscopy topography of the optimized cermet sample: anti-reflecting layer of ~110 nm Al_20_3/~70 nm Pt-Al_2O_3/~150 nm Mo/~0.5 mm Stainless steel substrate.

Figure 4 reports the crystallographic orientations of the optimized Al_2O_3/Pt-Al_2O_3/Mo/Stainless steel. Taking into account the anti-reflecting layer of Al_20_3, cermet layer of Pt-Al_2O_3 as well as the buffer IR reflective metallic layer of Mo is thin; the probing X-rays impinging the samples do penetrate and reach the stainless steel substrate. Indeed as shown by Figure 4, while the stainless steel substrate was highly crystalline with a net (111), (200) and (220) texturing, the buffer IR reflecting layer of Mo as well as the host Al_2O_3 matrix seemed to be fully amorphous as there was no corresponding Bragg peaks in the recorded 2Θ angular range of 30-80 deg. In contrast, and within the same angular range, one observes the (111), (200) and (220) Pt Bragg peaks. These peaks were quite wide corresponding to Pt grains with an average size "using the Debye-Scherer approximation" of about 3.2-4.7 nm in diameter hence corroborating with the values deduced from the SEM and AFM investigations within the error bars.

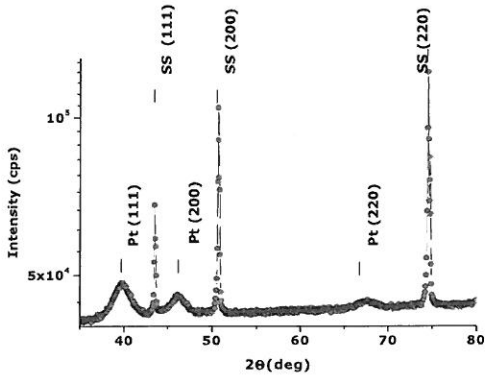

Figure 4. X rays diffraction patterns of the optimized cermet samples with and without the anti-reflecting layer of ~110 nm Al_2O_3/~70 nm Pt-Al_2O_3/~150 nm Mo/~0.5 mm Stainless steel substrate.

The optical reflectance spectra of simulated and experimental Pt-Al_2O_3 composites in the UV-VIS-NIR range of 300-2500 nm in particular for the Pt- Al_2O_3/Mo/Stainless steel substrate tandems without and with Al_2O_3 antireflection layer are shown in figure 5 (a) and (b) respectively. Hence the tandem without the Al_2O_3 anti-reflecting layer exhibited an absorptance of 0.93 and thermal emittance of 0.17, the corresponding one of the tandem with the Al_2O_3 anti-reflecting layer obtained an absorptance of 0.95 and thermal emittance of 0.11. The average total reflectance in the first spectral region was less than 10% it was decreased to 5% in the second one. These very low total reflectance values, which demonstrate the feasibility of the current considered optimized cermet based tandems, should be attributed not only to the optimized nature of the tandems with or without the Al_2O_3 reflecting layer but to the specific surface morphology and texture of these coatings as well.

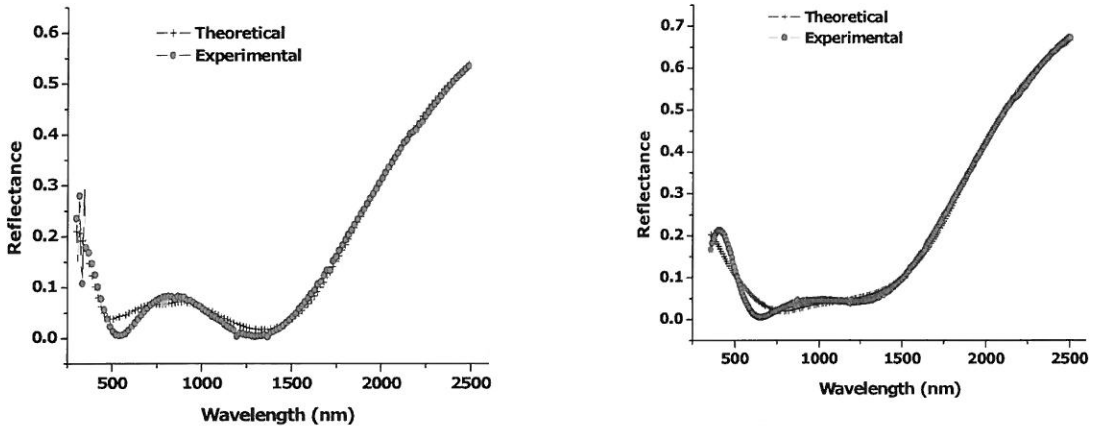

Figure 5. a) Experimental and calculated total Reflectivities "specular + non sepcular" of the optimized cermet samples without anti-reflection layer of ~70 nm Pt- Al_2O_3/~150 nm Mo/~0.5 mm Stainless steel substrate.

b) Experimental and calculated total Reflectivities "specular+ non sepcular" of the optimized cermet samples with anti-reflecting layer of ~110 nm Al_2O_3/~70 nm Pt- Al_2O_3/~150 nm Mo/~0.5 mm Stainless steel substrate.

4. Conclusion

In this work, optimized multilayered Pt-Al_2O_3 cermet nano-coatings onto Mo IR reflecting buffer layer coated stainless steel substrate with and without anti-reflecting layers of Al_2O_3 exhibited an excellent spectral selectivity of 0.95/0.11 which was consistent with a computer simulation. These cermet films are found to be thermally stable up to 650 °C in air. Combining such superior optical properties and the refractory nature of alumina as well as the chemical inertness of Pt, this type of coatings are competitive candidates for high temperature solar power plant applications.

Acknowledgment

We would like to thank for the finance support from (i) the Organization of Women Scientists for Developing World-Trieste "OWSDW", the Abdus Salam ICTP-Trieste, the Nanosciences African Network "NANOAFNET"-Cape Town, as well as iThemba LABS-National Research Foundation of South Africa.

References

[1] Granqvist C G 1991 J. Appl. Phys. A **52** 83
[2] Granqvist C G and Niklasson G A 1978 Phys. Rev. B **18** 554
[3] Niklasson G A and C G Granqvist 1984 J. Appl. Phys. **55** 3382
[4] Sella C and Lafait J 1988 J. Appl. Surf. Sci. **33/34** 942
[5]. Kenndy C E 2002 NREL/TP-520-31267
[6]. Thronton J A, Penfold A S and Lamb J L 1980 Thin Solid Films **72** 101
[7]. Berthier S, Lafait J, Sella C and Vien T K 1985 Thin Solid Films **125** 171
[8]. Maaza M, Nemraoui O, Sella C , Lafait J, Gibaud A, Pischedda V 2005 J. Phys. Letters A **344**
[9]. Sella C, Maaza M, Pardo B, Dunsteter F and Sainte Catherine M C 1997 J. Phys. A **241** 192
[10]. Gibaud A, Sella C, Maaza M, Sung L, Dura J A, Satija S.K 1999 Thin Solid Films **340** 153
[11]. Sella C, Maaza M, Pardo B, Dunsteter F, Martin J C and Kaba A 1997 J. Surface and Coatings Technology **97** 603
[12]. Maaza M, Nemraoui O, Sella C, Lafait J, Gibaud A, Baruch-Barak A and Beye A C 2006 J. Solid State Comms. **137** 166